Arch. Metall. Mater. **70** (2025), 2, 883-886

DOI: https://doi.org/10.24425/amm.2025.153490

TOMOO YOSHIDA[1*], SEUNGWON LEE[2], TAIKI TSUCHIYA[2],
SATOSHI MURAKAMI[2], KENJI MATSUDA[2]

EFFECT OF THE GRAIN BOUNDARY MICROSTRUCTURE ON SCC RESISTANCE OF HIGH STRENGTH Al-Zn-Mg ALLOY EXTRUDED MATERIALS

It is known while Al-Zn-Mg alloys extruded materials have high strength, those materials are characteristically occurred to Stress Corrosion Cracking (SCC). Our group have systematically controlled Mg and Zn composition and clarified the relationship between strength and precipitates. The purpose of this study is to clarify the relationship between the mechanical properties and SCC resistance and the microstructure. Therefore, our group controlled the mechanical properties and SCC resistance by adjusting the chemical composition and the quenching conditions of our Al-Zn-Mg alloy extruded materials, and the following two findings were obtained by using SCC test, tensile test, and transmission electron microscope (TEM) observation. The number density of η' phase on Al-Zn-Mg alloy extruded materials affected the improvement of mechanical properties, and the precipitation free zone (PFZ), which is the grain boundary microstructure affected SCC resistance.

Keywords: Al-Zn-Mg alloy; Stress Corrosion Cracking; microstructure

1. Introduction

Recently, the carbon neutral initiatives have been accelerated, and the automotive industry is promoting the reduction of CO_2 emissions based on life cycle assessments by changing internal combustion engine vehicles to battery electric vehicles, as typified by the "Electric (E)" in CASE [1]. Therefore, it is necessary for automobiles to install heavier battery packs.

The weight reduction of automobile body parts should be accelerated, and the application of aluminum alloys, such as diecasting aluminum alloys, rolled aluminum alloys, and extruded aluminum alloys, should be considered [2].

Al-Zn-Mg alloy extruded materials have high strength and high extrusion productivity [3,4]. Those are expected to adapt to bumper reinforcement, door beams and other applications materials. However, Al-Zn-Mg alloy extruded materials are more susceptible to Stress Corrosion Cracking (SCC) than other aluminum alloy extruded materials [5]. Our research group has systematically controlled Mg and Zn composition on Al-Zn-Mg alloys and clarified the relationship between strength and precipitates [6,7]. This study focuses on SCC in high-strength Al-Zn-Mg alloy extruded materials and investigates the relationship between SCC resistance and grain boundary microstructure. by a combination of chemical composition of alloys, quenching method, and stating temperature for water quenching after solid solution treatment.

2. Experimental procedures

The chemical composition of investigated alloys and production methods are presented in TABLES 1 and 2. Based on these, nine the samples with different characteristic were produced. The samples were melted and cast in the air and then homogenized at 748 K for 86.4 ks, and finally extruded to the plate shape. For all extruded the samples supersaturated solid solution treatment at 748 K for 3.6 ks was applied and quenched in water or specified conditions, and then aging treatment by tempering. TABLE 2 shows the quenching condition of all samples.

Tensile tests were performed at room temperature using Instron 5985 tensile testing machine. The tensile test specimens had parallel sections of 6.0 mm width, 0.8 mm thickness, and 17.5 mm length, or 12.5 mm width, 2 mm thickness, and 25 mm length.

[1] AISIN KEIKINZOKU CO., LTD, IMIZU, TOYAMA, JAPAN
[2] UNIVERSITY OF TOYAMA, FACULTY OF SUSTAINABLE DESIGN, TOYAMA, JAPAN

* Corresponding author: Tomoo-Yoshida@Aisin-Ak.Co.Jp

TABLE 1

The chemical composition of all samples

	Chemical composition (mass %)								
	Si	Fe	Cu	Mn	Mg	Zn	Zr	Ti	Al
Sample 1	0.05	0.17	0.25	0.25	1.71	6.75	0.18	0.02	bal.
Sample 2	0.00	0.00	0.46	0.00	3.51	4.72	0.00	0.00	bal.
Sample 3	0.00	0.00	0.00	0.00	3.42	9.21	0.18	0.02	bal.
Sample 4	0.00	0.00	2.18	0.00	1.70	8.92	0.18	0.02	bal.
Sample 5-9	0.03	0.15	0.20	0.19	1.92	7.04	0.14	0.03	bal.

TABLE 2

The quenching condition of all samples

	Solid solution treatment temperature (K)	Water quenching start temperature (K)	Note
Sample 1-4	773	—	Air quenching
Sample 5	773	773	Water quenching
Sample 6	773	673	
Sample 7	773	623	
Sample 8	773	573	
Sample 9	773	523	

SCC test specimens for 3-point bending were loaded by the stress of 180 MPa. Those specimens were immersed in a mixture of potassium dichromate, chromium oxide (IV), and sodium chloride for 28.8 ks at 363 to 373 K.

SCC effect was determined by observation with Keyence VHX-6000 digital microscope.

The microstructures by TEM were observed using Topcon EM-002B, acceleration voltage at 120 kV.

3. Results and discussion

3.1. Results of mechanical property measurements

Fig. 1 shows mechanical properties for all investigated samples.

Comparing the Samples 1 and 2, the Zn/Mg ratio is different, but the proof stress was mostly the same 500 MPa. The Zn/Mg ratio of the Samples 3 and 4 is also different from each other, but their proof stress was mostly the same 650 MPa. In the case of Samples 5-9, Zn/Mg ratio is almost the same, the water quenching start temperature is different, then their proof stress was changed.

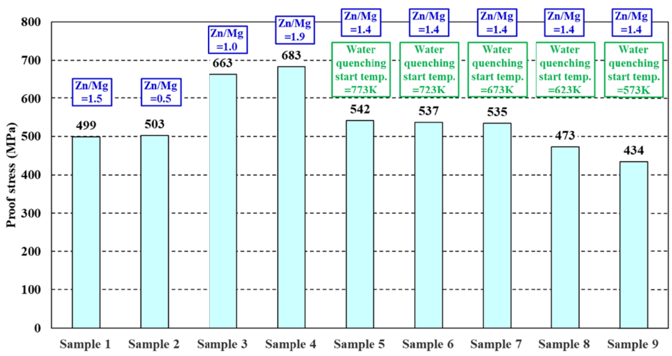

Fig. 1. The results of the mechanical properties of investigated samples

Proof stress was almost the same in water quenching start temperature from 773 K to 623 K.

Whereas, in water quenching start temperature is from 623 K to 523 K, that stress has trend to decreasing.

Fig. 2 shows TEM observation results performed inside a grain of the Samples 1 and 2. Both samples have proof stress of 500 MPa and numerous precipitates inside the grain characterised by the different contrast than Al-matrix. These precipitates are the most probably the η' phase, according to the analysis of the selected area electron diffraction (SAED) patterns. The number density of these η' phase on both the samples was about 15,000 μm^{-2}. The Samples 3-9 have different proof stress and numerous precipitates inside the grain as the same as the Sample 1 and 2. These precipitates are also probably η' phase by SAED pattern analysis.

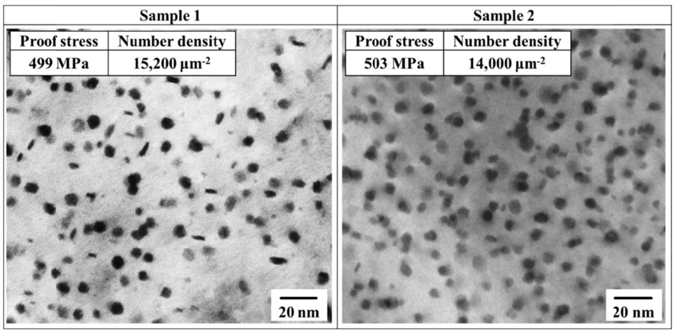

Fig. 2. TEM observation results inside grain on Sample 1 and Sample 2

Fig. 3 shows the relationship between the number density of η' phase precipitates and proof stress. As the number density of η' phase precipitates increases, proof stress would have an increased trend.

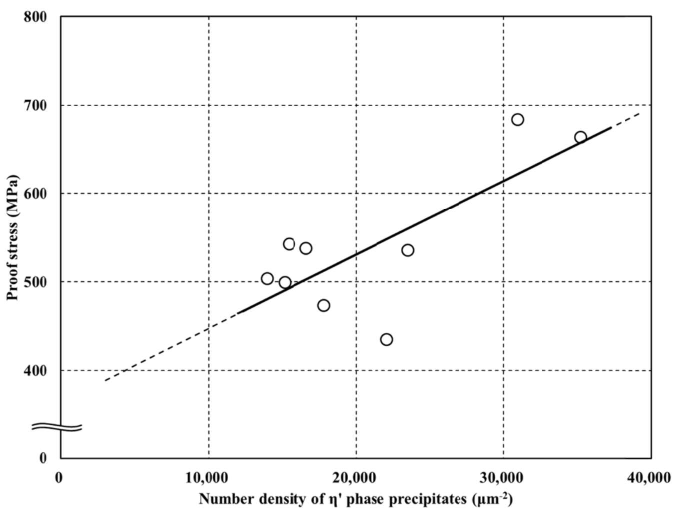

Fig. 3. The relationship between number density of η' phase precipitates inside grain and proof stress

3.2. Results of SCC investigation

Fig. 4 shows SCC test result of all samples. In the Sample 1 and in the Samples 7-9, the SCC is not present, therefore, these samples would have sufficient SCC resistance.

Whereas the Sample 2, 3, 4, 5, and 6 occurred the SCC effect. However, SCC resistance of the Sample 4 should be superior to the Samples 2, 3, 5 and 6.

Fig. 5 shows the optical microscope results of the Sample 1 and 2 microstructure observations. The Sample 1 has fibre structure and no crack after SCC test in observed. The Sample 2 has typical recrystallized microstructure characterised by coarse equiaxed grains with cracks occurred after 7.2 ks SCC test. The Sample 2 must have inferior SCC resistance to the Sample 1, because SCC occurs along coarse recrystallization grain boundaries.

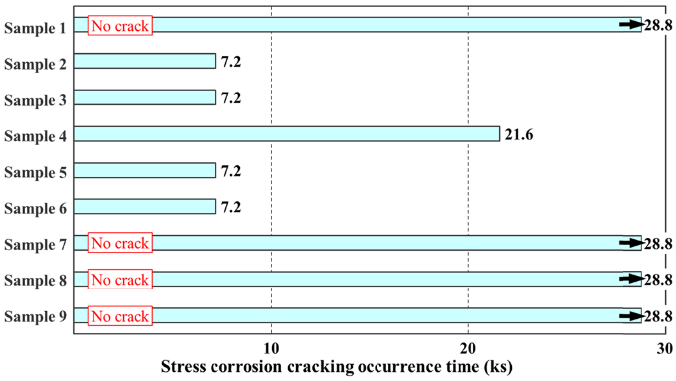

Fig. 4. The results of SCC test

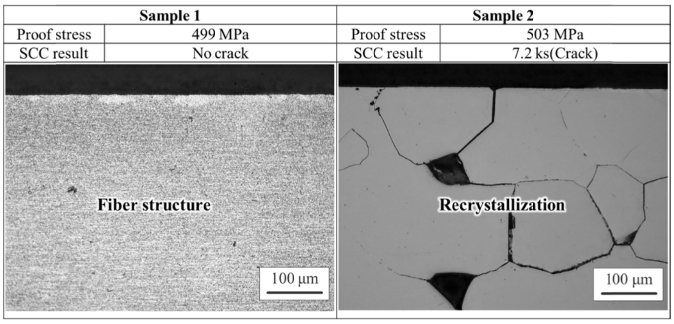

Fig. 5. OM observation of the Sample 1 and the Sample 2 after SCC test

Fig. 6 shows the optical microscope results of the Samples 3 and 4 of microstructure observations. Both samples have fibre structure and occurred SCC. Samples 3 and 4 occurred SCC after 7.2 ks and 21.6 ks during the SCC test observed, respectively. This means that the SCC resistance of Sample 4 should be superior to Sample 3.

Fig. 7 shows TEM observation on the grain boundary of the Sample 3 and 4 after SCC test in observed. These samples have PFZ and coarse precipitates on the grain boundary. The width of PFZ in Samples 3 and 4 have been measured and they have the mostly the same width of about 22 nm and about 25 nm, respectively. This means that TEM observations of those air-quenching samples cannot provide an efficient understanding of the relationship between SCC resistance and the width of PFZ. Therefore, PFZ on the grain boundary was performed for Samples 5-9 which have different quenching conditions.

Fig. 8 shows optical microscope and TEM observation result of the Sample 5 after SCC test.

The Sample 5 has fibre structure of crystal grains and occurred SCC after 7.2 ks SCC test, and it is the width of PFZ was about 20 nm.

As a result of investigating the Sample 6, 7, 8, and 9 by the same matter, PFZ of each sample are 6 nm, 27 nm, 16 nm, and 27 nm.

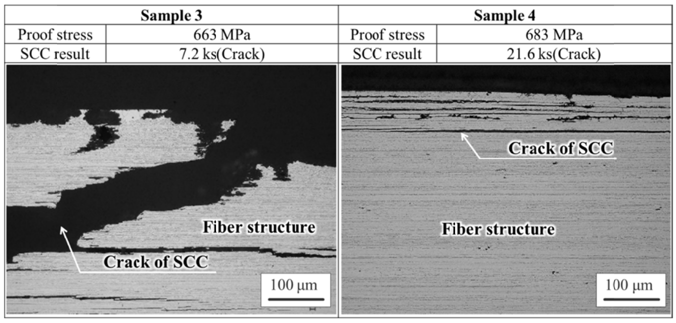

Fig. 6. OM observation of the Sample 3 and the Sample 4 after SCC test

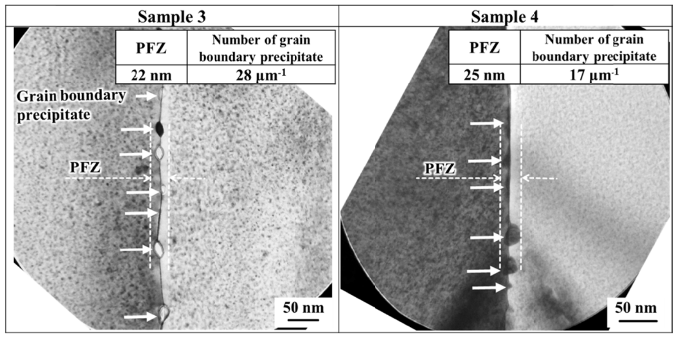

Fig. 7. TEM observation of the Sample 3 and the Sample 4 after SCC test

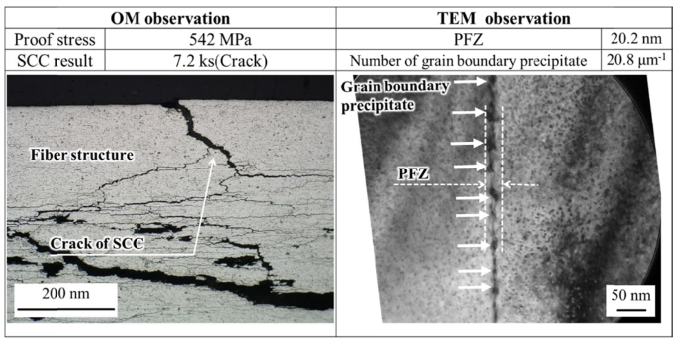

Fig. 8. OM observation after SCC test and TEM observation of the Sample 5

Fig. 9 shows the relationship between PFZ and SCC resistance.

As PFZ increases, SCC resistance shows an increased trend. In other word, the width of PFZ at grain boundary, which was formed by the different starting temperatures to water-quenching and aging treatment, affect SCC resistance.

It is known that SCC in Al-Zn-Mg alloys occurs when grain boundary precipitates are preferentially dissolved causing the potential difference between grain boundary precipitates and PFZ [5]. In this study, as shown in Fig. 9, as PFZ increases, SCC resistance would have increased trend, and it must be thought that the size and chemical composition of the dissolved grain boundary precipitates changed due to the chemical composition and the quenching conditions of our Al-Zn-Mg alloy extruded materials, and it should be presumed that the SCC property changed.

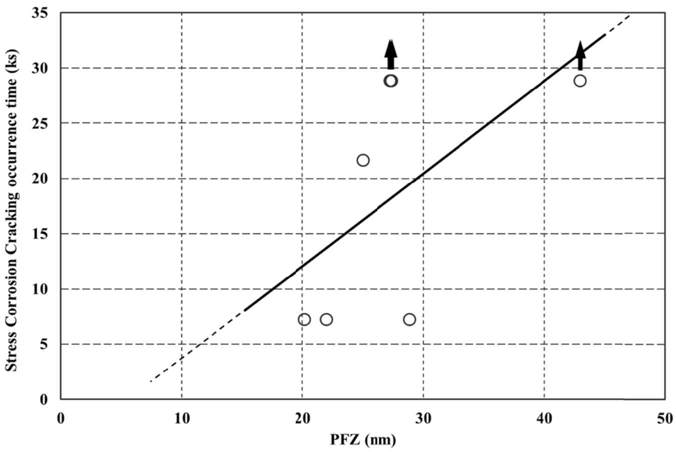

Fig. 9. The relationship between PFZ and SCC occurrence time

4. Conclusions

Our study obtained the following findings for Al-Zn-Mg alloy extruded materials by inves-tigating mechanical properties, SCC resistance and microstructure observation by TEM.

(1) Comparing the Samples 1 and 2, the Zn/Mg ratio is different, but the proof stress was mostly the same 500 MPa. The Zn/Mg ratio of the Samples 3 and 4 is also different from each other, but their proof stress was mostly the same 650 MPa. In the case of Samples 5-9, Zn/Mg ratio is almost the same, the water quenching start temperature is different, then their proof stress was changed.

(2) All samples have numerous precipitates inside the grain characterised by a different contrast than Al-matrix. These precipitates are the most probably the η' phase, according to the analysis of the SAED pattern.

(3) As the number density of η' phase precipitates increases, proof stress would have an increased trend in all of the conditions.

(4) As shown in Sample 1 and in the Samples 7-9, the SCC is not present. Therefore, these samples would have sufficient SCC resistance. Whereas samples 2-6 affected the SCC. However, the SCC resistance of Sample 4 was better than the other samples.

(5) As the width of PFZ increases, SCC resistance would have an increased trend. PFZ formed by the different starting temperatures to water-quenching and aging treatment would affect SCC resistance.

The results were presented during 14th Polish Japanese Joint Seminar on

Micro and Nano Analysis (3-6.09.2024, Toyama, Japan).

REFERENCE

[1] T. Nakanishi, CASE revolution-2030 Automobile Industry, Nikkei Inc. (2018).

[2] H.Hayashi, JILM **55**, 371-376 (2005).

[3] R. Akeret, P.M. Stratman, Unconventional Extrusion Processes for the Harder Aluminum Alloys, Part I, 15-18 (1973).

[4] R. Akeret, P.M. Stratman, Unconventional Extrusion Processes for the Harder Aluminum Alloys, Part II, 6-10 (1987).

[5] S. Ohsaki, Y. Kojima, T. Takahashi, JILM **30**, 694-700 (1980).

[6] K. Watanabe, K. Matsuda, N. Miura, Y. Uetani, S. Ikeno, T. Yoshida, S. Murakami, JILM **64**, 368-372 (2014).

[7] S. Lee, K. Watanabe, K. Matsuda, K. Nishimura, N. Nunomura, H. Toda, K. Hirayama, K. Shimizu, H. Gao, M. Yamaguchi, K. Ebihara, M. Itakura, T. Tsuru, T. Yoshida, S. Murakami, S.Ikeno, JILM **67**, 162-167 (2017).